



A fast SEVIRI simulator for quantifying retrieval uncertainties in the CM SAF cloud physical property algorithm

B. J. Jonkheid¹, R. A. Roebeling^{1,2}, and E. van Meijgaard¹

¹Royal Netherlands Meteorological Institute (KNMI), De Bilt, The Netherlands

²European Organisation for the Exploitation of Meteorological Satellites (EUMETSAT), Darmstadt, Germany

Correspondence to: B. J. Jonkheid (jonkheid@gmail.com)

Received: 26 August 2011 – Published in Atmos. Chem. Phys. Discuss.: 7 February 2012

Revised: 24 October 2012 – Accepted: 2 November 2012 – Published: 20 November 2012

Abstract. The uncertainties in the cloud physical properties derived from satellite observations make it difficult to interpret model evaluation studies. In this paper, the uncertainties in the cloud water path (CWP) retrievals derived with the cloud physical properties retrieval algorithm (CPP) of the climate monitoring satellite application facility (CM SAF) are investigated. To this end, a numerical simulator of MSG-SEVIRI observations has been developed that calculates the reflectances at 0.64 and 1.63 μm for a wide range of cloud parameter values, satellite viewing geometries and surface albedos using a plane-parallel radiative transfer model. The reflectances thus obtained are used as input to CPP, and the retrieved values of CWP are compared to the original input of the simulator. Cloud parameters considered in this paper refer to e.g. sub-pixel broken clouds and the simultaneous occurrence of ice and liquid water clouds within one pixel. These configurations are not represented in the CPP algorithm and as such the associated retrieval uncertainties are potentially substantial.

It is shown that the CWP retrievals are very sensitive to the assumptions made in the CPP code. The CWP retrieval errors are generally small for unbroken single-layer clouds with COT > 10, with retrieval errors of $\sim 3\%$ for liquid water clouds to $\sim 10\%$ for ice clouds. In a multi-layer cloud, when both liquid water and ice clouds are present in a pixel, the CWP retrieval errors increase dramatically; depending on the cloud, this can lead to uncertainties of 40–80%. CWP retrievals also become more uncertain when the cloud does not cover the entire pixel, leading to errors of $\sim 50\%$ for cloud fractions of 0.75 and even larger errors for smaller cloud fractions. Thus, the satellite retrieval of cloud physical properties of broken clouds as well as multi-layer clouds is complicated

by inherent difficulties, and the proper interpretation of such retrievals requires extra care.

1 Introduction

Clouds play a significant role in the climate system, since they influence the atmospheric energy balance by scattering and absorbing solar and terrestrial radiation, and by playing a key role in the atmospheric water cycle. Thus, it is important for climate models to treat clouds as accurately as possible. Comparison of model cloud physical properties with satellite observations is a valuable tool in providing accurate cloud statistics (Roebeling et al., 2006).

Comparing model output to satellite observations can be done along several different routes, illustrated in Fig. 1. In route I, the model cloud field is compared to the cloud parameters (e.g. cloud optical thickness – COT, particle effective radius (r_{eff}), cloud water path – CWP) retrieved from the satellite observations; any discrepancies between model and retrieved properties can be assigned to errors in these parameters, although differences in spatial and temporal resolutions can also be an issue. It is also difficult to disentangle model errors from retrieval errors. In route II, synthetic radiances are derived from the model cloud field to compare to the observed radiances; this route is relatively straightforward and bypasses the issue of retrieval errors of route I, but it is not clear in this route how to interpret differences between model and observations in terms of physical parameters. Collocation between model grid cells and satellite pixels also remains an issue. Route III compares the input to and output from a simulator of level 2 satellite products; comparison

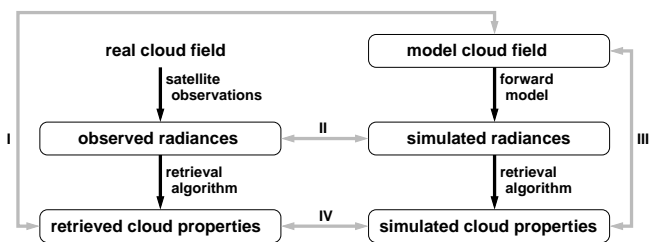


Fig. 1. Diagram of the comparison of climate model cloud fields with observations. The left side represents the observations of real clouds and the retrieval of satellite products, while the right side represents the model with simulated level 1 and level 2 satellite products. The boxes represent the available data sets, and the grey double-headed arrows represent routes along which comparisons can be performed between them. It should be noted that route III does not involve any reference to the real cloud field, but it is used to diagnose the climate model-forward model-retrieval chain.

between the input cloud parameters and the products is useful to diagnose the climate model-forward model-retrieval algorithm chain. In route IV, satellite products are simulated from the model output and compared to the observed products. This route has the same advantages as route II; moreover, differences between model output and satellite data are easier to interpret.

The classical methodology in model evaluation is to compare model fields directly with retrieved and collocated satellite products (i.e. route I in Fig. 1). Examples using this methodology are Molders et al. (1995), who evaluated cloud cover parametrization schemes with NOAA9 AVHRR data; Tselioudis and Jakob (2002) evaluated seasonal cloud property distributions of mid-latitude clouds in weather and climate models (ECMWF and GISS, respectively) with ISCCP observations; Roebeling and van Meijgaard (2009) evaluated diurnal variations in cloud physical properties by comparing statistics in model and satellite retrievals; and recently Greuell et al. (2011) evaluated a climate model using earth radiation budget observations from the GERB instrument and cloud physical properties from SEVIRI. The main disadvantage of such classical model evaluations is that model-to-satellite differences are partly due to model errors, partly due to inadequate satellite retrieval assumptions and finally due to intrinsic differences in the definitions of model and satellite products. Because of this entanglement of uncertainties in both the satellite retrievals and the model formulation of cloud parameters, it is difficult to assess model performance based on such an evaluation alone.

This paper aims to quantify the uncertainties in the cloud physical properties (CPP) retrieval algorithm of the climate monitoring satellite application facility (CM SAF), which uses the reflectances at 0.64 and 1.63 μm in the Nakajima and King (1990) method (see Fig. 2) to retrieve COT and r_{eff} , from which CWP can be calculated. The goal is to determine the circumstances under which the cloud properties

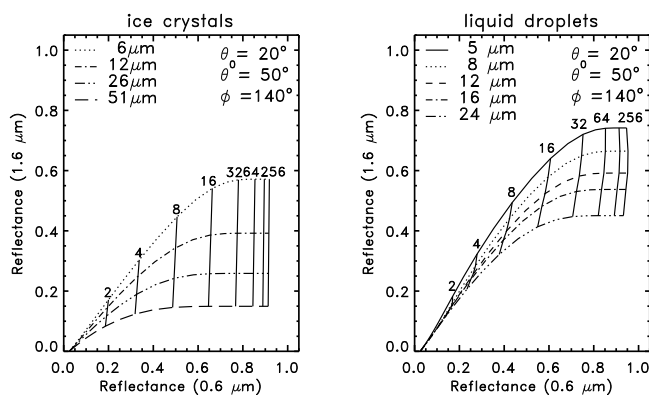


Fig. 2. The Nakajima and King (1990) retrieval method. Each curve shows the values of reflectances at 0.64 and 1.63 μm for a certain value of r_{eff} as a function of COT (indicated by the mostly vertical lines). Thus, from a combination of these reflectances both the COT and r_{eff} of a cloud can be determined. The left panel shows the retrieval curves for ice crystals, the right panel for water droplets; the viewing geometry is indicated in the upper right of each panel, with θ_0 the solar zenith angle, θ the satellite zenith angle and ϕ the relative azimuth angle. A surface albedo of 0 was used for these diagrams.

retrievals from the CPP algorithm are sufficiently reliable for classical model evaluations over a large domain (e.g. Europe), i.e. route I in Fig. 1. To achieve this goal, the approach indicated by route III in Fig. 1 is applied: the retrieval uncertainties are quantified in a systematic way by generating artificial cloudy scenes that vary with respect to three parameters that are known to affect the accuracy of Nakajima and King (1990) based retrievals: viewing geometry, fractional cloudiness and the presence of both ice and liquid water in one pixel.

To facilitate this study a simulator has been developed that is capable of generating cloud physical properties as retrieved by the CM SAF CPP algorithm. The simulator includes a forward model that projects the model predicted 3-D cloudy atmosphere onto a 2-D synthetic satellite image which contains information similar to observed satellite images inferred from measurements with the SEVIRI instrument. By using synthetic satellite data as input to the CPP algorithm, the cloud parameters obtained from simulated retrievals can be directly compared with the model predicted cloud parameters that served as an input to the simulator. Sampling many different cloud conditions allows a systematic assessment of the quality of the CPP algorithm for a large variety of cloudy atmospheres (cf. route III in Fig. 1). The simulator is designed to work on cloud fields produced by large-scale atmospheric models, e.g. (regional) climate models, operated at horizontal resolutions typically in the range from 10 to 100 km; in this study we adopted 25 km. The forward model then utilizes a decomposition of a climate model grid column into subcolumns with an effective

horizontal resolution of ~ 5 km. Choosing the 5 km scale is motivated by the consideration that effects of 3-D radiative transfer can safely be ignored at this scale, because such effects are known to be very small at scales beyond 1 km (Zinner and Mayer, 2006). Also the effect of the plane-parallel bias on cloud property retrievals from simulated radiances is supposedly small at the 5 km scale. Plane-parallel bias effects are negligible at the 1 km scale, while they are expected to play only a minor role at the ~ 5 km scale used in this study (Pincus et al., 1999)

The subject of this study has similarities with the study by Bugliaro et al. (2011) who used the radiances derived from a single model field generated with the regional consortium for small-scale modelling Europe (COSMO-EU) model. Their aim was to quantify errors in COT, r_{eff} and CWP retrievals from the algorithm for the physical investigation of clouds with SEVIRI (APICS) and the CPP algorithm. However, there are several differences in approach and methodology between their study and the one presented here. First, in the current paper the retrieval errors are analysed in a more systematic way with respect to the effects of viewing geometry, multi-layer clouds and broken clouds, aiming to span the entire input space of the simulator. In contrast, Bugliaro et al. (2011) focus more on the comparison of two cloud properties retrieval algorithms on the basis of a single 3-D COSMO-EU cloud field to generate different cloud conditions. Second, the forward model presented here uses a different radiative transfer model (i.e. the Doubling Adding KNMI (DAK) model, Stammes, 2001) than the forward model used by Bugliaro et al. (2011) (i.e. the libRadtran model, Mayer and Kylling, 2005). The latter influenced the comparison results of Bugliaro et al. (2011), because part of the differences they found can be attributed to radiative transfer model differences between the CPP and APICS algorithms. Since in the current paper the radiative transfer models of the forward model and retrieval algorithm are identical these differences play no role. A more detailed comparison of the results of these studies will be discussed in the body of this paper.

This paper is organised as follows: in Sect. 2 the SEVIRI instrument is introduced, and the simulator used in this work is described along with its components, the newly developed forward model and the CPP algorithm. Section 3 discusses the results of the study, and in Sect. 4 the conclusions and outlook are given.

2 Data and methods

2.1 The SEVIRI instrument

The Spinning Enhanced Visible and Infrared Imager (SEVIRI) is a passive imager that is flown onboard Meteosat Second Generation (MSG), a series of geostationary satellites that are operated by the European Organization for the Exploitation of Meteorological Satellites (EUMETSAT).

The SEVIRI instrument scans the complete disk of the Earth every 15 min, and operates three channels at visible and near infrared wavelengths between 0.6 and 1.6 μm , eight channels at infrared wavelengths between 3.8 and 14 μm , and one high-resolution visible channel. The nadir spatial resolution of SEVIRI is $1 \times 1 \text{ km}^2$ for the high-resolution channel, and $3 \times 3 \text{ km}^2$ for the other channels.

2.2 Simulator

Several simulators of satellite observations have already been developed, including the ISCCP simulator (Klein and Jakob, 1999; Webb et al., 2001; Tselioudis and Jakob, 2002), the EarthCARE simulator (Voors et al., 2007; Donovan et al., 2008), and the COSP simulator (Bodas-Salcedo et al., 2011). Simulators are generally built for different applications.

The International Satellite Cloud Climatology Project (ISCCP) simulator was developed to convert cloud and atmosphere information from atmospheric models directly into the cloud information that is produced by the ISCCP project. This project provides the first global climatology of cloud cover and cloud properties (including cloud optical thickness – COT, cloud top pressure and an estimate of cloud water path – CWP) at a spatial resolution of 280 km (Rossow and Garder, 1993; Rossow and Schiffer, 1999).

The EarthCARE simulator (ECSIM) is a computational tool which can simulate the complete EarthCARE mission. ECSIM generates ground- and space-based radar and lidar observations as well as the satellite observed radiances at the top of the atmosphere for the same cloud scenario. This simulator can simulate all the 4 instruments aboard the EarthCARE satellite, such as the 94 GHz cloud profiling radar, the high spectral resolution lidar at 353 nm, the multispectral imager and the broad-band radiometer. Cloud scenes, as input for the simulations, can be created using the embedded ECSIM cloud generator or they can be converted from Cloud Resolving Models or from Large Eddy Simulation models to ECSIM standard input. ECSIM is developed for the simulations of small scale cloud fields, typically $10 \times 10 \text{ km}^2$.

The CFMIP observation simulator package (COSP) was developed to convert climate model or mesoscale model output to observations of instruments on the A Train: the Cloud-Sat cloud profiling radar, the CALIPSO cloud and aerosol lidar and the MISR and MODIS instruments. The package also includes the ISCCP simulator.

It is also worth to note here the libRadtran software package, which was developed as a general atmospheric radiative transfer solver for wavelengths ranging from thermal infrared through the ultraviolet (Mayer and Kylling, 2005). The package includes a variety of solvers that can calculate radiances, irradiances or actinic fluxes in plane-parallel and pseudo-spherical 1-D systems, or full 3-D Monte Carlo calculations. The various solvers can incorporate ice and liquid water clouds, aerosols, Rayleigh scattering and molecular absorption; the surface is usually treated Lambertian,

although some solvers can also accommodate a specified surface BRDF. This package was used as a forward model for a retrieval algorithm sensitivity study by Bugliaro et al. (2011).

The aforementioned simulators are not applicable in practice for the study under consideration here, for which accurate top of the atmosphere radiance calculations are required over a large domain (at least Europe) within a reasonable time frame. The simulator should eventually be capable of running concurrently with a weather or climate model in order to facilitate real-time comparisons, or run it on a long span of climate model output to investigate its statistical properties. It consists of two parts: a forward model that accurately and efficiently calculate reflectances at visible and near-infrared wavelengths (specifically at 0.64 μm and 1.63 μm) for 3-D model cloud fields at regional to sub-global scales; and the CM SAF cloud physical properties (CPP) algorithm that retrieves COT and particle effective radius (r_{eff}) from these reflectances. CWP is then derived from the retrieved cloud properties.

2.2.1 Forward model

Online radiative transfer calculations were found to be too slow to be practical for the present study. To improve the computational speed of the forward model the radiative transfer is instead performed by scanning a lookup table (LUT) which has been set up in advance in a reduced parameter space. To use this lookup table the vertical structure in each computational gridbox is reduced to a handful of parameters that contain the essential information.

When working with a climate model, the forward model has to work with layers that are only partially cloudy. In such cases an independent column approximation is used with the stochastic cloud cover scheme by Räisänen et al. (2004) (see Fig. 3a). In this approach, a given grid box cloud cover profile is randomly distributed in a possible configuration of subcolumns, each of which is made up of either fully cloudy or cloud free layers (i.e. no partially cloudy layers in the subcolumns) with the constraint that summation over all subcolumns reconstructs the original cloud cover profile and cloud condensate distribution. The reflectance is calculated for each subcolumn independently, and the results are averaged to obtain the reflectance representative of the grid box. The number of subcolumns is taken as $n_{\text{sub}} = 20$ conform the argument pointed out in the introduction that the subcolumns should have an effective horizontal resolution of ~ 5 km. Further, each subcolumn has its vertical profiles of ice and liquid water content simplified to contain only the relevant information (see Fig. 3b): vertical profiles of water droplets and ice crystals, each with its own profile of r_{eff} , are reduced to two layers: a liquid water layer at 1–2 km and/or an ice layer at 5–6 km. Each layer is given the optical thickness of the integrated vertical profile corresponding to its phase. r_{eff} is uniform in each layer; for the current study r_{eff} is chosen in such a way that the layer has the same cloud water path

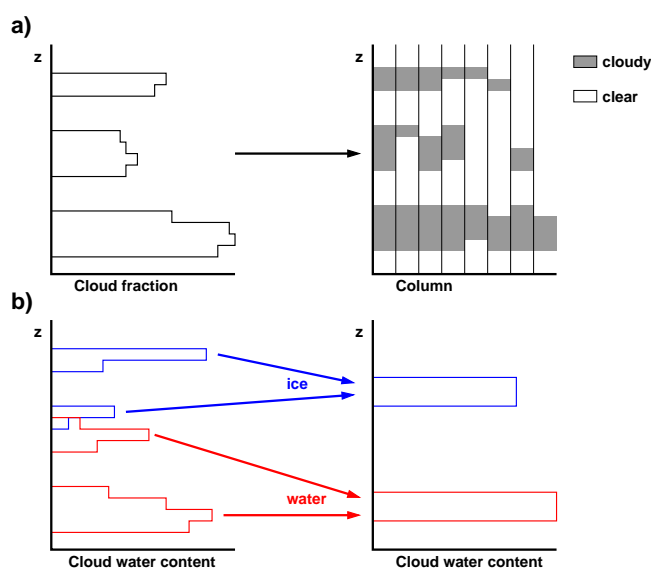


Fig. 3. Simplifications made to the cloud structure in the SEVIRI simulator: **(a)** each model grid cell is divided into subcolumns; in each subcolumn, a model layer that has a non-zero cloud fraction is either completely cloudy or completely clear following the stochastic method of Räisänen et al. (2004); **(b)** in each subcolumn all the ice is put into a single layer at 5–6 km, while all the liquid water is put into a single layer at 1–2 km.

as the vertical profile. For future applications that demand a more accurate representation of the model cloud reflectances, a more sophisticated value for r_{eff} will be used (several possibilities are offered by e.g. Platnick, 2000). If only a single thermodynamic phase is present in a given column, the calculations are performed for a single layer. The surface is always treated as a Lambertian reflector with the albedo at the different wavelengths given by the climate model, while the clouds are assumed to be in a standard mid-latitude summer atmosphere (Anderson et al., 1986).

The simplifications of the vertical cloud structure greatly speed up the radiative transfer calculations, but come at the cost of a decrease in accuracy. The exact cost is hard to ascertain, but based on a sampling of a model cloud field covering Europe (see also Sect. 3.2) the error introduced is of the order of ~ 5 %.

The reflectances of the clouds constructed in this way are calculated with DAK. The geometries at which DAK reflectances are calculated are on a slightly different grid than is used for the CPP LUTs. This was done to make sure that in the interaction between the two codes there is always a small error introduced by the interpolation on the LUT, which allows us to study trends in the error sensitivity even for cloud scenes where CPP should perform optimally. Note that although the LUTs of CPP and the simulator seem similar at a superficial level, the former does not allow both ice crystals and liquid water droplets to be present simultaneously

Table 1. Details of the lookup tables used in the forward model and the CPP retrieval algorithm.

	Forward model	CPP
Solar and satellite zenith angles θ_0, θ	0–75° (44 points)	0–75° (65 points)
Azimuthal angle ϕ	0–180° (91 points)	0–180° (91 points)
Total cloud optical thickness	0, 0.25–256 (22 points)	0, 0.25–256 (22 points)
Effective radius (ice crystals)	30–60 μm (3 points)*	6–51 μm (4 points)
Effective radius (liquid water droplets)	10–13 μm (2 points)*	1–24 μm (7 points)
Cloud composition	Up to two uniform layers	One uniform layer
Cloud height	1–2 km (liquid water droplets) 5–6 km (ice crystals)	1–2 km (all)

* The effective radius values in the forward model lookup table were chosen to reflect the range in values in the RACMO climate model.

whereas the latter does. Table 1 gives an overview of the characteristics of both lookup tables.

Once the cloud structure is simplified in this way, it can be parametrized with only four degrees of freedom: COT, optical ice fraction $f_{\text{ice}} = \text{COT}_{\text{ice}}/\text{COT}_{\text{total}}$, and r_{eff} of both liquid water droplets and ice crystals. Together with α_{surf} , solar and satellite zenith angles θ_0 and θ and sun-satellite azimuthal angle ϕ , this gives an 8-D lookup table from which the reflectances at 0.64 μm and 1.63 μm can be interpolated. This lookup table is summarised in Table 1. Interpolation is done linearly, except for α_{surf} , for which the equation by Chandrasekhar (1960) was used:

$$R(\alpha_{\text{surf}}) = R(\alpha = 0) + \frac{\alpha_{\text{surf}} t(\theta_0) t(\theta)}{1 - \alpha_{\text{surf}} \alpha_{\text{hemi}}}$$

where R is the reflectance at the top of the atmosphere, $t(\theta_0)$ and $t(\theta)$ denote the atmospheric transmissions at solar and satellite zenith angles, and α_{hemi} is the hemispherical sky albedo for upwelling isotropic radiation. Note that the α_{hemi} and the product $t(\theta_0)t(\theta)$ are not independently given in the lookup table, but calculated from the reflectances at surface albedo 0, 0.5 and 1.

It should be noted that the choices made in the forward model, for example when it comes to ice crystal phase functions or 1-D versus 3-D radiative transfer calculations, can have a profound effect on the interaction with the retrieval algorithm in a sensitivity study (cf. route III in Fig. 1). If the assumptions made in the respective codes are different, it is hard to interpret any differences in the outcome of the study as being due to inherent limitations in the retrieval algorithm.

2.2.2 Cloud physical properties retrieval algorithm

The parameters COT, r_{eff} and CWP are retrieved with the cloud physical properties algorithm (CPP) developed at the Royal Netherlands Meteorological Institute (KNMI) within the climate monitoring satellite application facility (CM SAF) of EUMETSAT (Roebeling et al., 2006). The CPP algorithm retrieves these properties from visible, near-infrared and infrared radiances observed by passive imagers, such as

the SEVIRI instrument onboard MSG, the Advanced Very High Resolution Radiometer (AVHRR) onboard the National Oceanic and Atmospheric Administration (NOAA) satellites, or the Moderate Resolution Imaging Spectroradiometer (MODIS) on board EOS Aqua or Terra.

The Nakajima and King (1990) method is used to retrieve COT and r_{eff} for cloudy pixels in an iterative manner by simultaneously comparing satellite observed reflectances at visible (0.6 μm) and near-infrared (1.6 μm) wavelengths to look-up tables (LUTs) of simulated reflectances of liquid water and ice clouds for given optical thicknesses, particle sizes and surface albedos (α_{surf}). The retrieval of cloud thermodynamic phase (ice or liquid water) is done simultaneously with the retrieval of COT and particle size. The ice phase is assigned to pixels for which the observed 0.6 and 1.6 μm reflectances correspond to simulated reflectances of ice clouds, and the cloud top temperature determined from the 10.8 μm channel is lower than 265 K. The remaining cloudy pixels are considered to represent liquid water clouds (Wolters et al., 2008). Note that the retrieval of r_{eff} at low values of COT is complicated by the limited variation of the reflectance at 1.6 μm (cf. Fig. 2). For clouds with $\text{COT} < 8$ the final value for r_{eff} is relaxed by weighting the value derived with the Nakajima and King (1990) method and a climatological average value (8 μm for liquid water clouds or 26 μm for ice clouds), where the weight assigned to the climatology increases linearly from 0 at $\text{COT} = 8$ to 1 at $\text{COT} = 0$. This is done to avoid spuriously strong variations in the outcome of r_{eff} . All clouds are assumed to be in a layer between 1 and 2 km height in a standard mid-latitude summer atmosphere taken from Anderson et al. (1986).

Assuming vertically homogeneous clouds, the CWP is computed from the retrieved COT and r_{eff} using $\text{CWP} = 4/3 \text{COT} r_{\text{eff}}/Q_{\text{ext}}$, where Q_{ext} is the extinction efficiency $Q_{\text{ext}} = \sigma_{\text{ext}}/\pi r_{\text{eff}}^2$ and σ_{ext} the extinction cross section of liquid water droplets or ice crystals of the appropriate size. It should be noted that Q_{ext} is almost uniformly two for droplets, so the expression simplifies to $\text{CWP} = 2/3 \text{COT} r_{\text{eff}}$, while for ice crystals it can range from two for small r_{eff} to 1.5 for larger crystals. The retrievals are limited

to satellite and solar viewing zenith angles smaller than 72° . At larger solar and viewing zenith angles the errors in the retrievals are too large due to the decreased accuracy of the radiative transfer simulations, the decreased signal to noise ratio of the reflectance observations, and the increased 3-D radiative effects (Várnai and Marshak, 2007).

The LUTs have been generated with the Doubling Adding KNMI (DAK) radiative transfer model (Stammes, 2001). The optical thicknesses range from 0 to 256. Cloud droplets are assumed to be spherical with effective radii between 1 and $24\ \mu\text{m}$. For ice clouds, imperfect hexagonal ice crystals (Hess et al., 1998) are assumed with radii between 6 and $51\ \mu\text{m}$. Note that r_{eff} is defined slightly differently for ice crystals and liquid water droplets: for ice crystals, the volume equivalent radius for a hexagonal column r_{vol} is used, while the radii of liquid water droplets are assumed to follow a gamma distribution with an effective variance of 0.15; the effective radius is defined as $r_{\text{eff}} = \langle r^3 \rangle / \langle r^2 \rangle$, with $\langle \dots \rangle$ denoting an average over the size distribution.

The MODTRAN model (Berk et al., 2000) is used to calculate, and correct for, the absorption by atmospheric trace gases on band-averaged reflectances as observed by satellite instruments (Meirink et al., 2009). The surface reflectance maps have been generated from five years of MODIS white-sky albedo data (Moody et al., 2008). The algorithm to separate cloud free from cloud contaminated and cloud filled pixels originates from the MODIS cloud detection algorithm (Ackerman et al., 1998; Platnick et al., 2003; Frey et al., 2008). It has been modified to make it applicable to other passive imagers and to make it independent from ancillary data (Roebeling et al., 2008).

3 Results and discussion

3.1 Testing the CPP retrieval algorithm

To investigate the validity of the CPP retrieval algorithm, the simulator is used to obtain reflectances for a variety of input parameters. These reflectances are then used as input data of the CPP algorithm, and the retrieved cloud physical properties are compared to the original input. The emphasis is on the retrieval of CWP, using the retrievals of COT and r_{eff} only as intermediate steps. This choice was made because CWP is a prognostic variable in climate models, while COT is usually derived from an assumed r_{eff} . Therefore, looking at retrieval errors of COT and r_{eff} is of limited relevance when the underlying purpose is to gauge the usefulness of CPP in model evaluation, and they will only be mentioned in relation to CWP retrievals.

Despite the fact that the forward model is built to calculate radiances from climate model output, no actual climate model data was used in the following evaluation of CPP. Instead, the choice was made to take advantage of the computational speed of the forward model to sample the input

Table 2. Parameter space explored in the CPP test in Sect. 3.

Parameter	Range
θ, θ_0	$0-72^\circ$, in intervals of 0.05 in $\cos(\theta)$
ϕ	$0-180^\circ$, in intervals of 4.5°
COT	0.8–204.8, in factors of 2
f_{ice}^*	0, 0.02, 0.05, 0.2, 0.4, 0.8, 1
α_{surf}	0.05, 0.1, 0.2, 0.4, 0.8
Cloud fraction*	0.125–1, in intervals of 0.125

* f_{ice} is only varied for clouds with cloud fraction = 1; cloud fraction is only varied for pure water clouds.

space of the simulator and perform retrievals on the resulting radiances. Thus all cloud configurations that are possible in the set-up of the forward model are studied, even unphysical ones, instead of relying on a climate model field to provide the necessary variation in clouds. The parameter space for this test is summarised in Table 2.

In the following sections, both multi-layer clouds (i.e. cloudy pixels containing both ice clouds and liquid water clouds) and clouds containing only one layer of either ice or liquid water (labeled “pure ice” and “pure liquid water”) are studied, even though the latter two cases represent ideal situations where CPP should perform optimally; in fact, the only significant source of uncertainties in this regime is the retrieval of r_{eff} at low values of COT. The reason for this is twofold: first, the single-phase simulations provide a baseline error analysis with which other effects can be compared; for instance, retrievals of r_{eff} become uncertain for low values of COT, and this will be reflected in the analysis of single-phase clouds. Second, some sources of retrieval errors such as large solar zenith angles or broken clouds become more apparent if single-phase clouds are considered because these effects can then be considered the only sources of uncertainty.

3.1.1 Effects of solar zenith angle

As a first test the influence on the solar zenith angle θ_0 on the CWP retrieval is examined for pure ice and pure liquid water clouds with a COT of either 6.4 or 102.4; α_{surf} was 0.1 in all cases, while the effective radii of droplets and ice crystals are kept fixed at $11\ \mu\text{m}$ and $38\ \mu\text{m}$, respectively. The resulting CWP retrieval errors, averaged over all satellite viewing angles with $\theta < 72^\circ$ on a grid consisting of 14 points in θ (equidistant in $\cos(\theta)$) and 41 equidistant points in ϕ , are shown in Fig. 4. Three measures for the retrieval errors are used:

- the mean relative error, which indicates the bias of the retrievals, defined as $(\langle \text{CWP} \rangle - \text{CWP}^*) / \text{CWP}^*$,
- the RMS relative error, which indicates the accuracy of the retrievals, defined as $\sqrt{(\langle (\text{CWP} - \text{CWP}^*)^2 \rangle)} / \text{CWP}^*$,

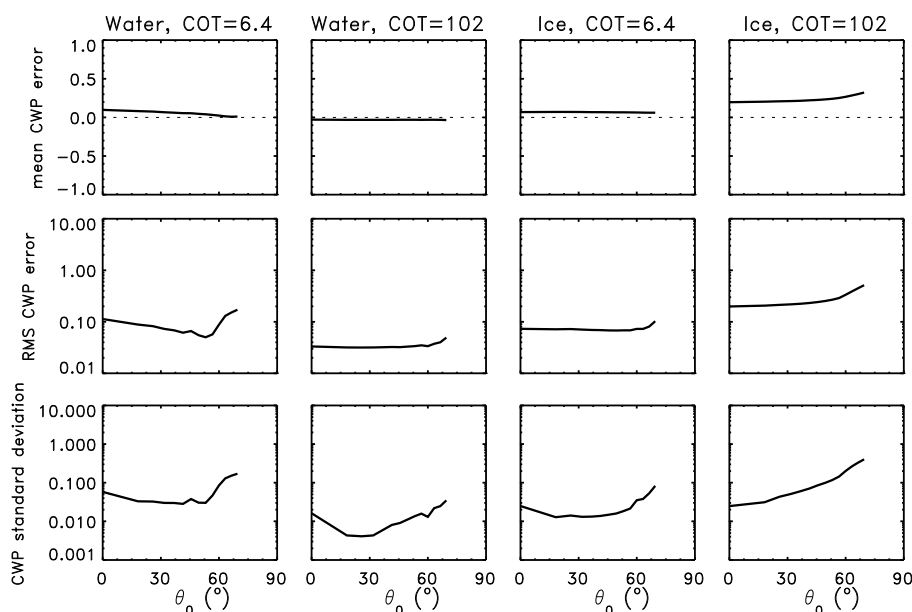


Fig. 4. The CWP retrieval errors as a function of solar zenith angle θ_0 , for different pure liquid water and pure ice clouds (indicated at the top of each column). The top row shows the mean relative error (indicative of the bias of the retrievals); the middle row shows the RMS relative error (indicative of the accuracy of the retrievals); the lower row shows the standard deviation (indicative of the precision of the retrievals). Results were averaged over all satellite geometries with $\theta < 72^\circ$; the effective radii are $r_{\text{eff}} = 11 \mu\text{m}$ for liquid water clouds and $r_{\text{eff}} = 38 \mu\text{m}$ for ice clouds.

- the relative standard deviation, which indicates the precision of the retrievals, defined as $\sqrt{\langle (CWP - \langle CWP \rangle)^2 \rangle} / CWP^*$,

where $\langle \dots \rangle$ denotes a mean over the relevant geometries, CWP denotes the retrieved values as a function of geometry for a given cloud configuration, and CWP* denotes the input value for this cloud configuration, which is independent of the geometry. Thus, the quantities are given as dimensionless numbers, relative to the input CWP. In all cases the errors are averaged over all satellite geometries with $\theta < 72^\circ$, which is the largest zenith angle where CPP can still do meaningful retrievals.

It can be seen that liquid water clouds have generally low retrieval errors in these circumstances for most solar zenith angles. This is to be expected: the conditions for the radiative transfer calculations used here are almost identical to those used in the CPP algorithm, except for the values of r_{eff} and sun-satellite geometry used in the respective lookup tables; the different grids introduce slight interpolation errors with respect to each other. There is an additional source of errors in the retrieval of the low COT clouds; due to uncertainties in the retrieval of r_{eff} at low optical thickness (cf. Fig. 2), CPP uses a weighted mean of the retrieved r_{eff} and a climatological mean of $8 \mu\text{m}$ for liquid water droplets and $26 \mu\text{m}$ for ice crystals. This causes a relatively low standard deviation in the retrievals, but the bias it introduces leads to RMS errors of the order of 10%. At large solar zenith an-

gles ($\theta_0 > 60^\circ$) retrievals become more problematic and less precise as a consequence. At higher COT values this effect disappears, since it is easier to retrieve r_{eff} there. The CWP retrieval errors for thin ice clouds mirror those of liquid water clouds. At large solar zenith angles, there is a predominantly positive retrieval error in the forward scattering direction, while mainly negative for backscatter. For thick ice clouds, the CWP retrieval errors are larger than for liquid water clouds. This is caused by an overestimation of COT due to a combination of two effects: first, the ice clouds in the simulator are at 6 km, while CPP assumes all clouds to be at 2 km; this causes slight differences in the Rayleigh scattering occurring above the cloud, and hence different reflectances at $0.6 \mu\text{m}$. The second effect can be seen in Fig. 2, where the reflectances at $0.6 \mu\text{m}$ for ice clouds saturate at a relatively low reflectance due to the small asymmetry factors of the Hess et al. (1998) ice crystals.

3.1.2 Effects of COT, multi-layer clouds and surface albedo

For a more thorough investigation of the effects of COT, α_{surf} and multi-layer clouds (parametrised by the optical ice fraction f_{ice}), the reflectances are calculated for a parameter space spanning the relevant values of these parameters. This parameter space consists of a grid of 9 values of COT (ranging from 0.8 to 204.8), 7 values of f_{ice} (pure ice and pure liquid water clouds, plus five intermediate points ranging from $f_{\text{ice}} = 0.02$ to 0.8) and 5 values of α_{surf} (ranging from 0.05

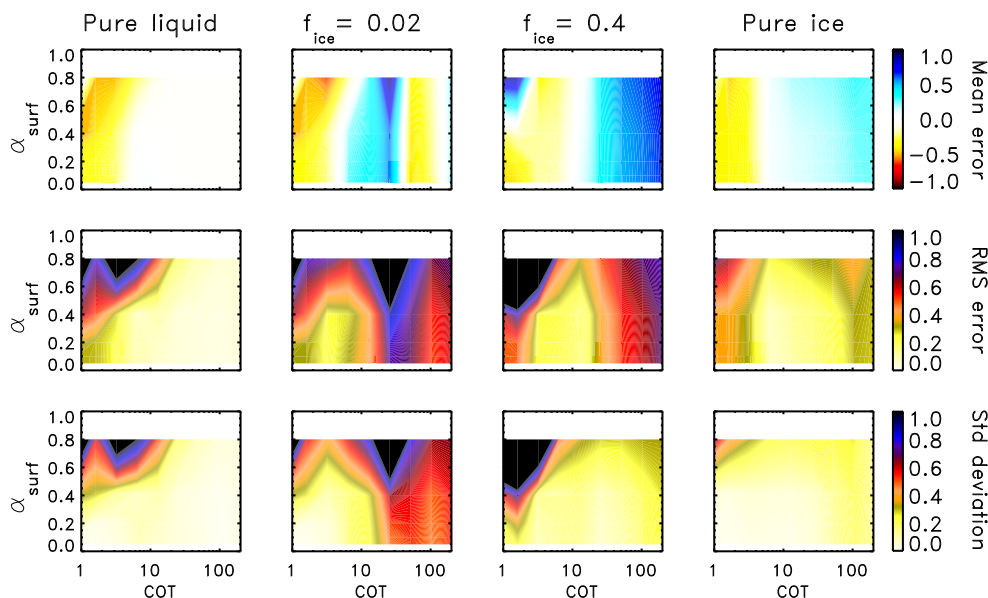


Fig. 5. The CWP retrieval errors as a function of COT and α_{surf} , averaged over all satellite viewing angles with $\theta < 72^\circ$ and solar zenith angles with $\theta_0 < 72^\circ$. The columns indicate different values of f_{ice} , while the rows are as in Fig. 4. Again, effective radii are $r_{\text{eff}} = 11 \mu\text{m}$ for liquid water clouds and $r_{\text{eff}} = 38 \mu\text{m}$ for ice clouds.

to 0.8); for simplicity the same α_{surf} values are used at both 0.6 and $1.6 \mu\text{m}$. Again, the effective radii of ice crystals and liquid water droplets are taken as $38 \mu\text{m}$ and $11 \mu\text{m}$, respectively, and are assumed to be uniform within the cloud.

The CWP retrieval errors are illustrated in Figs. 5 and 6. As before, the retrieval errors are averaged over all satellite viewing angles with $\theta < 72^\circ$; now they are also averaged over all solar zenith angles with $\theta_0 < 72^\circ$ to focus more on the effects of the cloud and surface properties. It can be seen that retrieval errors are generally small for pure liquid water clouds, and to a lesser extent for pure ice clouds, generalising the results illustrated in Fig. 4. The only exceptions occur for low COT, caused by the aforementioned use in CPP of climatological mean values of r_{eff} , and for ice clouds with an optical thickness $\gtrsim 10$, caused by the fact that the simulator uses a different cloud top height from the CPP algorithm for ice clouds. As a result the COT retrievals for pure ice clouds are generally too high and quickly approach 256, the maximum COT value that CPP can retrieve. This explains the relatively high precision of the retrievals, and why the retrieval errors decrease as the input COT approaches this maximum value.

Varying the surface albedo has a limited effect on the CWP retrieval quality, increasing the uncertainties only at very high values ($\alpha_{\text{surf}} > 0.5$, i.e. snow-covered surfaces). For these bright surfaces the retrieval of COT becomes problematic because the contrast between the cloud and the surface decreases, leading to an overestimation of COT. The uncertainties decrease for $\text{COT} > 10$, where the surface albedo has little influence on the reflectances. For very high values of COT, the CPP algorithm tends to yield $\text{COT} = 256$, the

maximum value in the CPP LUTs; this reinforces the relatively low retrieval uncertainties regardless of surface albedo as the actual COT approaches this upper limit.

Retrievals of CWP are of a much lower quality in the case of multi-layer clouds, due to various reasons. The root of this problem is that CPP only defines a single phase for each retrieval, meaning it cannot interpret multi-layer clouds correctly. Even a thin ice cloud layer over a liquid water cloud layer can already introduce a large retrieval error: if the ice layer has enough optical thickness (typically with $\text{COT}_{\text{ice}} > 1$) the phase retrieval will interpret the entire COT of both layers as an ice cloud; even if the ice layer is optically thin, the different phase function of the ice crystals will introduce errors in the retrieval when a pure liquid water cloud is assumed. This is illustrated in the second and third columns of Fig. 5, and in Fig. 6: for low values of f_{ice} (i.e. a thin ice cloud over a thick liquid water cloud), the CWP retrieval has the smallest error if the ice layer is still translucent (i.e. $\text{COT}_{\text{ice}} \ll 1$) and the phase retrieval is made for the bulk of the cloud. As the optical thickness of the ice layer increases, the ice crystals contribute more and more to the total cloud reflectance, interfering with the retrievals. This mixing of phase functions causes the largest errors in the second column of Fig. 5, around $\text{COT} = 20\text{--}30$, or in the third columns around $\text{COT} = 2$, and also accounts for the peaks in the first two columns of Fig. 6 around $f_{\text{ice}} = 0.15$. When the ice layer becomes optically thick the retrieval errors of COT decrease, because the cloud's reflectance matches with the retrieved cloud phase. In Figs. 5 and 6 the fact that the ice layer becomes optically thick, and the corresponding switch

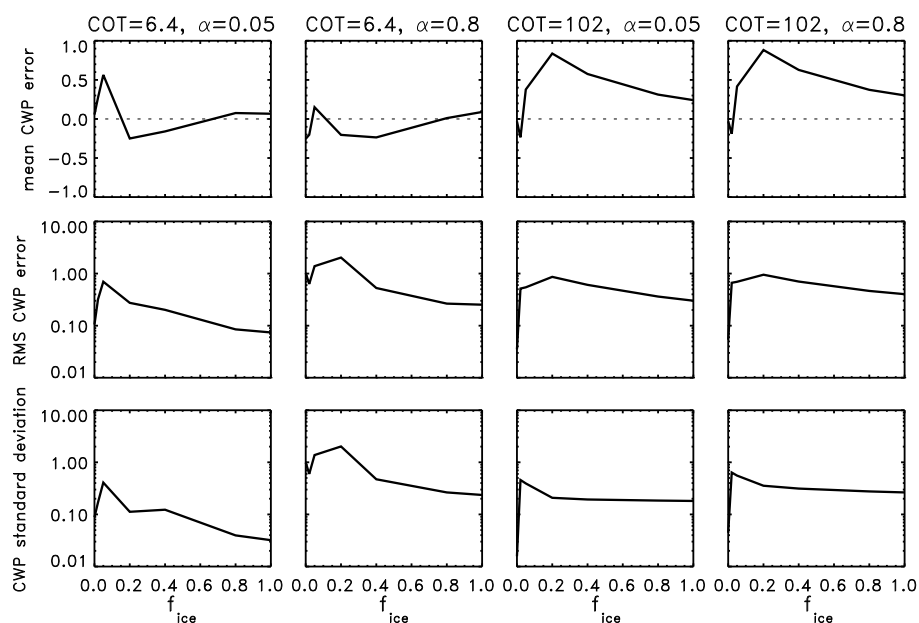


Fig. 6. As Fig. 4, except the errors are shown as functions of f_{ice} for several combinations of COT and α_{surf} .

to a different CPP LUT, shows as a sign change in the mean error. The CWP errors in that regime are mainly caused by the mismatch between retrieved and bulk cloud values of r_{eff} . For larger values of f_{ice} the errors are lower, since the retrieved phase represents a greater part of the total cloudy column.

3.1.3 Effects of fractional cloud cover

If a cloud is observed by the satellite, it will not necessarily fill the entire field of view. In general, a pixel that is interpreted as cloudy will have cloudy and clear parts, introducing uncertainties in the retrievals; specifically, r_{eff} is usually overestimated (Wolters et al., 2010; Zhang and Platnick, 2011) while COT and CWP are underestimated (Coakley et al., 2005). By construction this complication does not occur when simulating climate model fields, since the procedure outlined in Sect. 2.2 and Fig. 3 ensures that each sub-column used in the calculations is either completely cloudy or completely clear; yet since it may occur in the observations, the uncertainties introduced when retrieving CWP for partially clouded pixels have to be assessed.

To study the effect of partial cloud cover in a pixel, the reflectances were calculated for a fully covered cloudy field and a clear sky field; a weighted mean of the results (weighted according to the required cloud cover) was then used as the reflectance of the partially cloudy field. From these reflectances the CWP retrieval error is determined. This procedure was performed for liquid water clouds with various values for COT, α_{surf} and cloud cover; pure liquid water clouds are chosen because they have the smallest intrinsic retrieval errors, hence the resulting errors can be considered

to be mostly due to the fractional cloud cover. The resulting CWP retrieval errors are shown in Figs. 7 and 8. It can be seen that CWP retrieval errors rise dramatically for clouds with a relatively low COT or with very high COT, even at cloud fractions of 87.5 %. Only clouds with COT = 10–20 over a dark surface have low retrieval errors; for these clouds, the overestimation of r_{eff} is found to compensate the underestimation of COT. Retrieval errors tend to increase even further with decreasing cloud fraction, going to RMS errors of order unity for a cloud cover of 12.5 %. Retrievals of CWP are generally too low due to underestimations of COT at low α_{surf} , and of r_{eff} at high α_{surf} . The only exception occurs at low COT and high α_{surf} , where the bright surface complicates COT retrievals with a high chance of overestimations. It should be noted that the standard deviation of the retrievals is relatively low for cloud covers > 50 %, regardless of almost any variation in COT or α_{surf} . Thus it is at least theoretically possible to compensate for the retrieval errors introduced by fractional cloud cover if the cloud fraction is known somehow. An exception occurs for thin clouds (COT < 10) over a bright surface ($\alpha_{surf} > 0.5$), where CWP retrievals are problematic in any case (cf. Fig. 5).

3.2 Application to a climate model

A possible application of this work is to provide an uncertainty analysis on model cloud fields that one wants to compare with satellite data. To illustrate this, the simulator was used to obtain artificial SEVIRI observations and subsequent retrievals of a single climate model field using the Regional Atmospheric Climate Model (RACMO). RACMO is a hydrostatic limited-area model used for regional climate

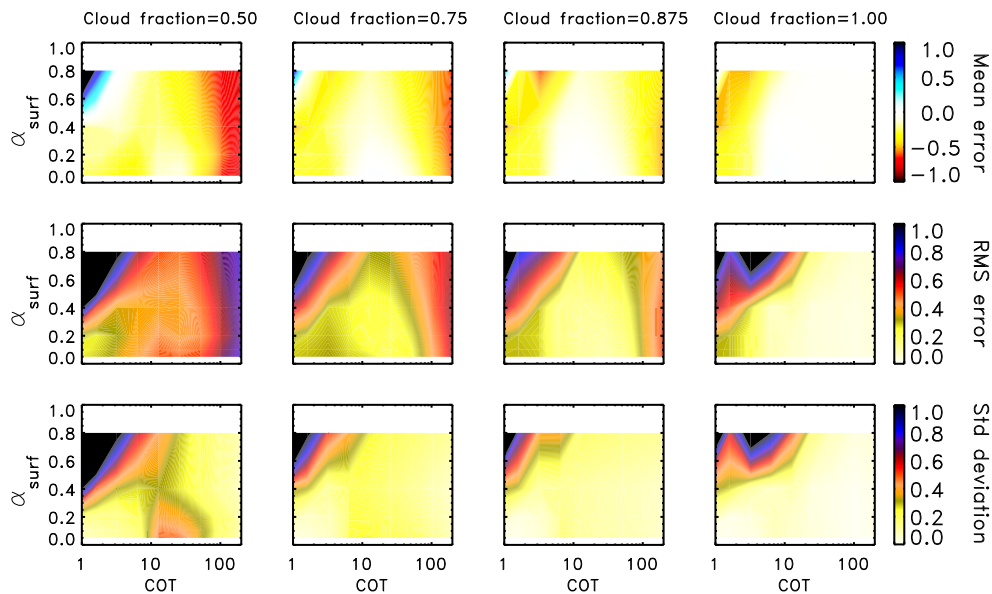


Fig. 7. As Fig. 5, except the results are for pure liquid water clouds, and the columns indicate different values of the cloud fraction.

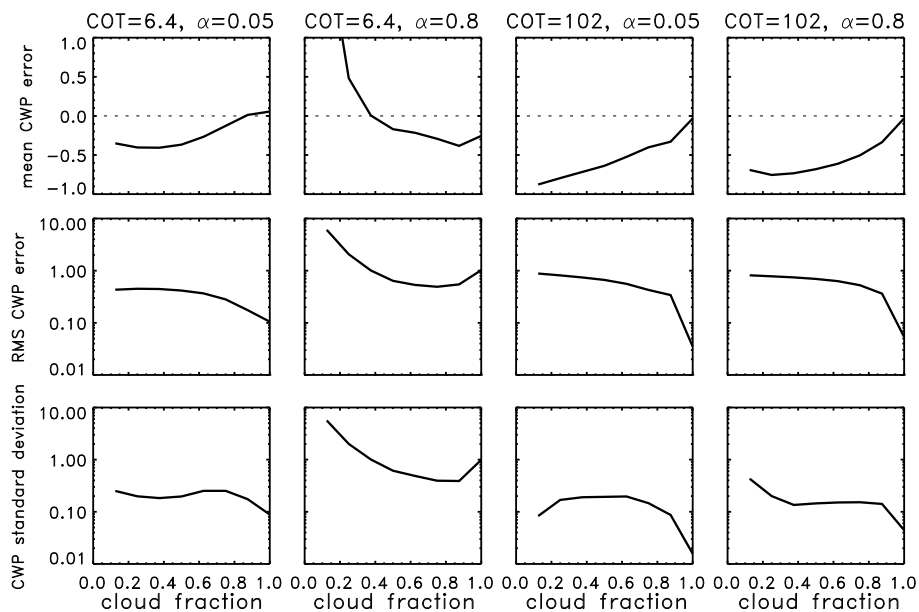


Fig. 8. As Fig. 6, except the errors are shown as functions of the cloud fraction for several combinations of COT and α_{surf} .

modeling; it has been developed at KNMI by porting then physics package of the ECMWF IFS (European Center for Medium-Range Weather Forecast Integrated Forecasting System), release cy23r4, into the forecast component of the HIRLAM (High Resolution Limited Area Model) NWP, version 5.0.6 (de Bruijn and van Meijgaard, 2005; van Meijgaard et al., 2008).

Figure 9 shows how the uncertainty analysis procedure is applied to a RACMO field across Western Europe, on 15 May 2009 at 12:00 UTC. For simplicity, the surface albedo

used in this test at both 0.64 and 1.63 μm is adopted from the RACMO value for short-wave radiation. It is notable that most of the clouds in this scene, and nearly all clouds with an appreciable CWP, have both liquid water and ice phase represented. This can also be seen in the reflectances, where the clouds which contain ice show up as dark structures in the 1.63 μm channel while the liquid water clouds are brighter due to their smaller r_{eff} . However, this means that both the relative and absolute retrieval errors are generally large throughout the domain. This fact can be seen in the

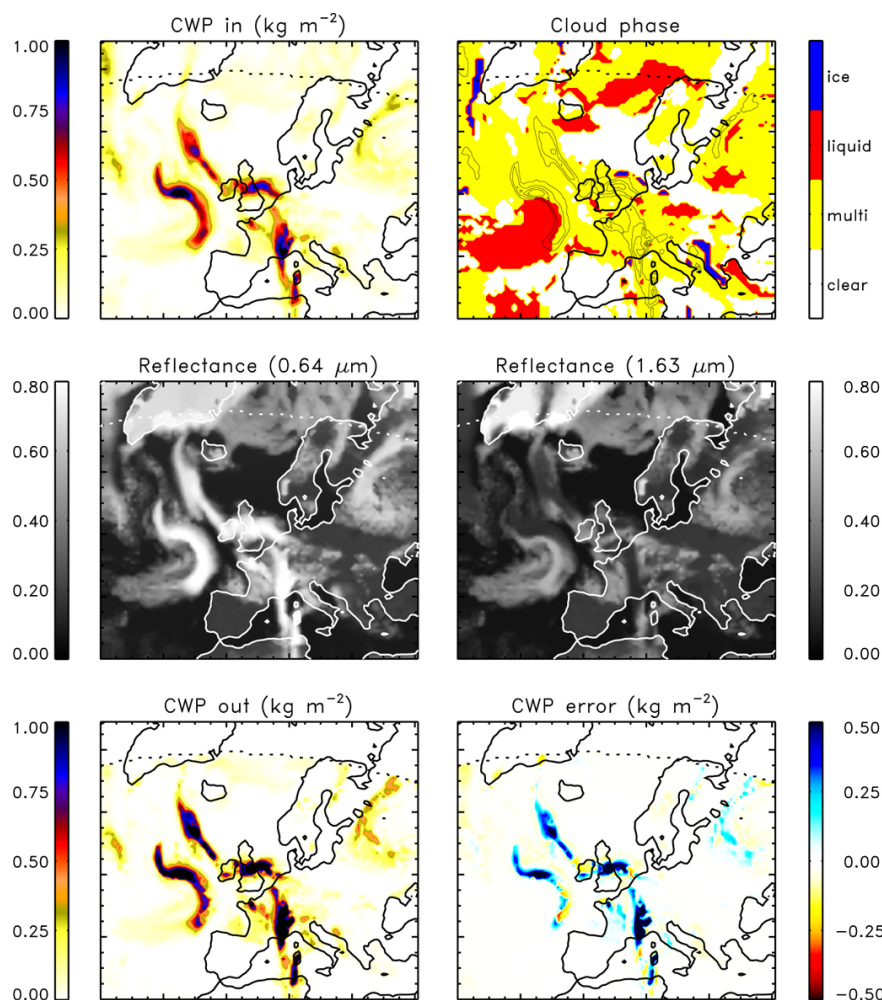


Fig. 9. Application of the simulator to a single RACMO field, for 15 May 2009, 12:00 UTC. The upper left panel gives the CWP calculated by RACMO; the upper right panel gives the cloud phase at each grid point ($> 99\%$ ice, $> 99\%$ liquid water, multi-layer, or clear), with contours tracing CWP for ease of reference; the center left panel gives the simulated reflectance at $0.64\ \mu\text{m}$; the center right panel gives the simulated reflectance at $1.63\ \mu\text{m}$; the lower left panel gives the retrieved CWP after the RACMO output was put through the simulator and CPP; the lower right panel gives the difference between the retrieved CWP and the RACMO CWP. In all panels the dotted line marks the area where both the solar and satellite zenith angles are less than 72° ; no retrievals are done beyond this line.

lower two panels of Fig. 9 where it is shown that nearly all clouds have their CWP overestimated by CPP. Notable exceptions occur in the pure liquid water clouds north west of the Iberian peninsula. As such, large differences between SEVIRI retrieved and model predicted CWP can be expected in those areas, even if the climate model were a perfect representation of reality. This result also emphasises that an evaluation of this model with satellite data should be conducted in the routes II or IV of Fig. 1, rather than route I.

3.3 Comparison with other studies

The results of this study contrast with the findings of Bugliaro et al. (2011), who performed a similar study on the retrieval errors of COT, r_{eff} and CWP. In their paper, the libRadtran 1-D radiative transfer solver was used to calculate

all the low-resolution SEVIRI channels for a single down-scaled 3-D cloud field produced by the COSMO-EU numerical weather prediction model. The retrieval errors were quantified by comparing the cloud properties retrieved by the CPP and the APICS algorithms, both applied to the synthetic SEVIRI reflectances, to the cloud properties in the COSMO-EU field.

One of the striking differences between their study and the present one is the much larger uncertainties Bugliaro et al. (2011) find for CPP retrievals of CWP. For liquid water clouds, they find a very broad distribution of differences between predicted and retrieved CWP values, with a width greater than the retrieved values and a tendency towards overestimation. This broad distribution of differences is most likely caused by uncertainties in the r_{eff} retrievals. This is

mainly due to the abundance of optically thin clouds in their sample: for liquid water clouds, they have a mean COT of 9.13, so a sizeable portion of the clouds have COT values much smaller than 8. For these thin clouds, CPP will nudge its r_{eff} retrievals towards a climatological mean of $8 \mu\text{m}$; combined with a mean r_{eff} in the model field of $5.32 \mu\text{m}$ this will result in a positive bias in the CWP retrievals. In the current paper it is shown that CPP has large retrieval errors for liquid water clouds with $\text{COT} < 5$, but performs well for greater optical thicknesses. The bias shown in Fig. 5 is negative due to the choice of $r_{\text{eff}} = 11 \mu\text{m}$ in these calculations, but has the same origins as the positive bias in Bugliaro et al. (2011). For the thicker clouds, differences in the CWP uncertainties may also be caused by the assumptions made in each simulator and its interaction with CPP; for instance, the forward model presented here places liquid water clouds at 2 km height in a model atmosphere, as does CPP, whereas Bugliaro et al. (2011) allow for variable cloud top heights.

Another difference between the two studies occurs with the CWP retrieval of ice clouds. This is again caused by low optical depth effects; for ice clouds the mean COT is 2.15, making this effect even more pronounced than for liquid water clouds. The mean r_{eff} is $41.32 \mu\text{m}$, meaning that the assumption in CPP of a climatological mean value of $26 \mu\text{m}$ for optically thin ice clouds can explain the underestimation of CWP. Also, their simulator uses different phase functions for ice crystals than CPP, while in the current paper the same type of crystals are used (albeit with different values of r_{eff}). For multi-layer clouds the two studies agree that CWP retrieval uncertainties are relatively large.

It is noteworthy that the APICS retrievals shown in Bugliaro et al. (2011) are generally more accurate and precise than the CPP retrievals. While the present paper offers no such comparison, it should be noted that the two studies are not neutral with respect to the retrieval algorithm used. Both APICS and the forward model applied in Bugliaro et al. (2011) are based on the libRadtran radiative transfer model, while both CPP and the forward model developed here are based on the DAK code. This set-up likely influences the interactions between the forward models and the retrieval algorithms, for example in the ice crystal scattering phase functions and the droplet size distribution.

4 Conclusions

Retrievals of cloud water path (CWP) with the CPP algorithm work well for pixels that are completely covered by either pure ice or pure liquid water clouds with cloud optical thickness $\text{COT} > 5$. For ice clouds, the retrieval error is within 10 % when $\text{COT} < 80$; liquid water clouds have comparable retrieval errors up to $\text{COT} = 200$. A very high surface albedo (> 0.5) leads to larger uncertainties. The CWP retrieval errors show little variation for $\theta_0 < 50^\circ$, and tend to increase for larger values of θ_0 .

For multi-layer clouds, CWP retrievals become very sensitive to errors when there is a thin ice cloud overlying a thick liquid water cloud. With such multi-layer clouds, an acceptable retrieval of CWP can only be carried out for very low values of the optical ice fraction f_{ice} , where the ice layer is optically thin and does not interfere with the observation of the liquid water layer, and for high values of $f_{\text{ice}} (> 0.6)$, where the ice layer represents the majority of the observed cloud. These uncertainties arise from the fact that the CPP cloud phase retrievals focus on a few optical depths at the top of the cloud; in carrying out a CWP retrieval it applies this information to the whole cloud using the method outlined in Sect. 2.2.2.

When a cloud covers only part of the SEVIRI pixel, the CWP retrievals show a considerable negative bias for cloud fractions $< 80\%$. The precision in the retrievals is quite good, however, indicating that the effects of broken cloud cover can be compensated if the cloud fraction is known somehow.

While some of the results presented here initially seem to contrast with the findings of Bugliaro et al. (2011), who performed a similar study, these discrepancies can be explained by differences in the experimental set-ups and assumptions that go into the respective simulators.

Acknowledgements. This work is part of the project titled “Construction and application of an MSG/SEVIRI simulator” that is carried out in the User Support Programme Space Research under the supervision of the Netherlands Space Office (NSO). We wish to thank Piet Stammes for the use of the DAK radiative transfer code. We would also like to thank Brent Maddux, Piet Stammes, Wouter Greuell and Jan Fokke Meirink for reviewing earlier versions of this manuscript. Further, we thank Jérôme Riédi for providing the SEVIRI cloud detection code, and Olaf Tuinder for his help with technical issues.

Edited by: B. Mayer

References

- Ackerman, S., Strabala, K., Menzel, W., Frey, R., Moeller, C., and Gumley, L.: Discriminating clear sky from clouds with MODIS, *J. Geophys. Res.*, 103, 32141–32157, 1998.
- Anderson, G., Clough, S., Kneizys, F., Chetwynd, J., and Shettle, E.: AFGL atmospheric constituent profiles (0–120 km), Tech. Rep. AFGL-TR-86-0110, Air Force Geophysics Laboratory, 1986.
- Berk, A., Anderson, G., Acharya, P., Chetwynd, J., Bernstein, L., Shettle, E., Matthew, M., and Adler-Golden, S.: MODTRAN4 Version 2 Users Manual, Tech. Rep., Air Force Research Laboratory, 2000.
- Bodas-Salcedo, A., Webb, M. J., Bony, S., Chepfer, H., Dufresne, J.-L., Klein, S., Zhang, Y., Marchand, R., Haynes, J. M., Pincus, R., and John, V. O.: COSP: Satellite simulation software for model assessment, *B. Am. Meteorol. Soc.*, 92, 1023–1043, 2011.

- Bugliaro, L., Zinner, T., Keil, C., Mayer, B., Hollmann, R., Reuter, M., and Thomas, W.: Validation of cloud property retrievals with simulated satellite radiances: a case study for SEVIRI, *Atmos. Chem. Phys.*, 11, 5603–5624, doi:10.5194/acp-11-5603-2011, 2011.
- Chandrasekhar, S.: *Radiative Transfer*, Dover Publications, 1960.
- Coakley, J., Friedman, M., and Tahnk, W.: Retrieval of cloud properties for partly cloudy imager pixels, *J. Atmos. Ocean. Tech.*, 22, 3–17, 2005.
- de Bruijn, E. and van Meijgaard, E.: Verification of HIRLAM with ECMWF physics compared with HIRLAM reference versions, HIRLAM Tech. Rep. 63, available from SMHI, S-601 76 Norrköping, Sweden, 2005.
- Donovan, D., Voors, R., van Zadelhoff, G.-J., and Acarreta, J.: EC-SIM Models and Algorithms Document, Tech. Rep., 2008.
- Frey, R., Ackerman, S., Liu, Y., Strabala, K., Zhang, H., Key, J., and Wang, X.: Cloud detection with MODIS. Part I: Improvements in the MODIS Cloud Mask for Collection 5, *J. Atmos. Ocean. Tech.*, 25, 1057–1072, 2008.
- Greuell, W., van Meijgaard, E., Meirink, J., and Clerbaux, N.: Evaluation of model predicted top-of-atmosphere radiation and cloud parameters over Africa with observations from GERB and SEVIRI, *J. Climate*, 24, 4015–4036, 2011.
- Hess, M., Koelemeijer, R., and Stammes, P.: Scattering matrices of imperfect hexagonal crystals, *J. Quant. Spectrosc. Ra.*, 60, 301–308, 1998.
- Klein, S. and Jakob, C.: Validation and sensitivities of frontal clouds simulated by the ECMWF model, *Month. Weather Rev.*, 127, 2514–2531, 1999.
- Mayer, B. and Kylling, A.: Technical note: The libRadtran software package for radiative transfer calculations – description and examples of use, *Atmos. Chem. Phys.*, 5, 1855–1877, doi:10.5194/acp-5-1855-2005, 2005.
- Meirink, J., Roebeling, R., and van Meijgaard, E.: Atmospheric correction for the KNMI cloud physical properties retrieval algorithm, Tech. Rep. TR-304, KNMI, 2009.
- Molders, N., Laube, M., and Raschke, E.: Evaluation of model generated cloud cover by means of satellite data, *Atmos. Res.*, 39, 91–111, 1995.
- Moody, E., King, M., Schaaf, C., and Platnick, S.: MODIS-Derived Spatially Complete Surface Albedo Products: Spatial and Temporal Pixel Distribution and Zonal Averages, *J. Appl. Meteor. Climatol.*, 47, 2879–2894, 2008.
- Nakajima, T. and King, M.: Determination of the Optical Thickness and Effective Particle Radius of Clouds from Reflected Solar Radiation Measurements. Part I: Theory, *J. Atmos. Sci.*, 47, 1878–1893, 1990.
- Pincus, R., McFarlane, S., and Klein, S.: Albedo bias and the horizontal variability of clouds in subtropical marine boundary layers: Observations from ships and satellites, *J. Geophys. Res.*, 104, 6183–6191, 1999.
- Platnick, S.: Vertical photon transport in cloud remote sensing problems, *J. Geophys. Res.*, 105, 22919–22935, 2000.
- Platnick, S., King, M., Ackerman, S., Menzel, W., Baum, B., Riedi, J., and Frey, R.: The MODIS cloud products: algorithms and examples from Terra, *IEEE T. Geosci. Remote Sens.*, 41, 459–473, 2003.
- Räisänen, P., Barker, H., Khairoutdinov, M., Li, J., and Randall, D.: Stochastic generation of subgrid-scale cloudy columns for large-scale models, *Q. J. Roy. Meteor. Soc.*, 130, 2047–2067, 2004.
- Roebeling, R. and van Meijgaard, E.: Evaluation of the daylight cycle of model predicted cloud amount and condensed water path over Europe with observations from MSG-SEVIRI, *J. Climate*, 22, 1749–1766, 2009.
- Roebeling, R., Feijt, A., and Stammes, P.: Cloud property retrievals for climate monitoring: implications of differences between Spinning Enhanced Visible and Infrared Imager (SEVIRI) on METEOSAT-8 and Advanced Very High Resolution Radiometer (AVHRR) on NOAA-17, *J. Geophys. Res.*, 111, D20210, doi:10.1029/2005JD006990, 2006.
- Roebeling, R., Deneke, H., and Feijt, A.: Validation of cloud liquid water path retrievals from SEVIRI using one year of CLOUDNET observations, *J. Appl. Meteor. Climatol.*, 47, 206–222, 2008.
- Rossow, W. and Garder, L.: Cloud detection using satellite measurements of infrared and visible radiances from ISCCP, *J. Climate*, 6, 2341–2369, 1993.
- Rossow, W. and Schiffer, R.: Advances in understanding clouds from ISCCP, *B. Am. Meteorol. Soc.*, 80, 2261–2287, 1999.
- Stammes, P.: Spectral radiance modeling in the UV-Visible range, in: *IRS 2000: current problems in atmospheric radiation*, edited by: Smith, W. and Timofeyev, Y., A. Deepak Publ., Hampton, Va, 385–388, 2001.
- Tselioudis, G. and Jakob, C.: Evaluation of midlatitude cloud properties in a weather and a climate model: dependence on dynamical regime and spatial resolution, *J. Geophys. Res.*, 107, 4781, doi:10.1029/2002JD002259, 2002.
- van Meijgaard, E., van Uft, L., van de Berg, W., Bosveld, F. C., van den Hurk, B., Lenderink, G., and Siebesma, A.: The KNMI regional atmospheric climate model RACMO version 2.1, Tech. Rep. TR-302, KNMI, 2008.
- Várnai, T. and Marshak, A.: View angle dependence of cloud optical thickness retrieved by MODIS, *J. Geophys. Res.*, 112, D06203, doi:10.1029/2005JD006912, 2007.
- Voors, R., Donovan, D., Acarreta, J., Eisinger, M., Franco, R., Lajas, D., Moyano, R., Pirondini, F., Ramos, J., and Wehr, T.: ECSIM: the simulator framework for EarthCARE, in: *Proc. SPIE 6744*, 2007.
- Webb, M., Senior, C., Bony, S., and Morcrette, J.-J.: Combining ERBE and ISCCP data to assess clouds in the Hadley Centre, ECMWF and LMD atmospheric climate models, *Clim. Dynam.*, 17, 905–922, 2001.
- Wolters, E., Roebeling, R., and Feijt, A.: Evaluation of cloud-phase retrieval methods for SEVIRI on Meteosat-8 using ground-based lidar and cloud radar data, *J. Appl. Meteor. Climatol.*, 47, 1723–1738, 2008.
- Wolters, E., Deneke, H., van der Hurk, B., Meirink, J., and Roebeling, R.: Broken and inhomogeneous cloud impact on satellite cloud particle effective radius and cloud-phase retrievals, *J. Geophys. Res.*, 115, D10214, doi:10.1029/2009JD012205, 2010.
- Zhang, Z. and Platnick, S.: An assessment of differences between cloud effective particle radius retrievals for marine water clouds from three MODIS spectral bands, *J. Geophys. Res.*, 116, D20215, doi:10.1029/2011JD016216, 2011.
- Zinner, T. and Mayer, B.: Remote sensing of stratocumulus clouds: Uncertainties and biases due to inhomogeneity, *J. Geophys. Res.*, 111, D14209, doi:10.1029/2005JD006955, 2006.